Pre-print Manuscript of Article:
Bridgelall, R., Huang, Y., Zhang, Z., Deng, F., "Precision enhancement of pavement roughness localization with connected vehicles," *Measurement Science and Technology*, 27(2016) 025012 (9pp), January 4, 2016.

Precision enhancement of pavement roughness localization with connected vehicles

R Bridgelall[1], Y Huang[2], Z Zhang[2], and F Deng[2]
[1*]Upper Great Plains Transportation Institute, North Dakota State University, Fargo, ND, USA
[2]Civil and Environmental Engineering Dept., North Dakota State University, Fargo, ND, USA

E-mail: raj@bridgelall.com

Abstract. Transportation agencies rely on the accurate localization and reporting of roadway anomalies that could pose serious hazards to the traveling public. However, the cost and technical limitations of present methods prevent their scaling to all roadways. Connected vehicles with on-board accelerometers and conventional geospatial position receivers offer an attractive alternative because of their potential to monitor all roadways in real-time. The conventional global positioning system is ubiquitous and essentially free to use but it produces impractically large position errors. This study evaluated the improvement in precision achievable by augmenting the conventional geo-fence system with a standard speed bump or an existing anomaly at a pre-determined position to establish a reference inertial marker. The speed sensor subsequently generates position tags for the remaining inertial samples by computing their path distances relative to the reference position. The error model and a case study using smartphones to emulate connected vehicles revealed that the precision in localization improves from tens of metres to sub-centimetre levels, and the accuracy of measuring localized roughness more than doubles. The research results demonstrate that transportation agencies will benefit from using the connected vehicle method to achieve precision and accuracy levels that are comparable to existing laser-based inertial profilers.

Keywords: accelerometer, connected vehicles, global positioning system, inertial profiler, pavement roughness localization, potholes, smartphone

1. Introduction

Localized roughness from anomalies such as frost heaves, pavement cracking, potholes, spills, and debris pose serious hazards to the traveling public. Hence, transportation agencies must rely on the regular and accurate reporting of localized roughness to prioritize maintenance needs (Karamihas and Senn 2012). The inaccurate reporting of anomaly positions or their mischaracterizations could lead to costly decisions or maintenance actions that are unnecessary. Some level of roughness is acceptable from pavement joints, patches, utility covers, rail grade crossings, and bridge sections. To enforce measurement precision and accuracy requirements, some agencies penalize contractors for erroneously reporting localized roughness (Chen and Dye 2014).

The international roughness index (IRI) is the prevalent method of summarizing pavement roughness (Gillespie *et al*. 1986). The IRI is an accumulation of the suspension motion of a fixed quarter-car (known as the Golden Car) simulated to traverse a sample of the elevation profile at a precise reference speed of 80 km h^{-1}. Nearly all transportation agencies currently use laser-based inertial profilers to measure the elevation profile of paved roadways (Merritt *et al*. 2014). To localize pavement sections with high-accuracy, technicians install a high-reflectivity adhesive tape to mark their boundaries. The adhesive tape reflects laser light with a high intensity to produce artificial maxima in the recorded elevation profile. Subsequent processing uses the signal maxima to isolate profile sections that are associated with the target segments. The operating guidelines for laser-based inertial profilers specify a 25-mm sample interval along the elevation profile (Gillespie *et al*. 1986). Therefore, the precision bounds of its localization must be within that interval.

Although using inertial profilers to produce the IRI is now common practice, practitioners are aware of the numerous shortcomings. Researchers have long discovered that the IRI mischaracterizes roughness that riders experience because of the fixed Golden Car parameters and the precise reference speed (Ahlin and Granlund 2002) (Papagiannakis 1997) (Lak *et al*. 2011). Furthermore, most implementations of inertial profilers are difficult or impractical to apply on unpaved, urban, and local roads where they must avoid frequent anomalies and stop-and-go conditions (NCHRP 2013). These deficiencies coupled with the relatively high cost to acquire, maintain, and operate inertial profilers have motivated agencies to seek alternative methods.

The United States Department of Transportation (USDOT) and equivalent agencies worldwide are collaborating with nearly all vehicle manufacturers to deploy connected vehicle pilots in major cities and to assure that they will become pervasive by 2020 (USDOT 2015). The connected vehicle standard prescribes architectures and methods that would allow remote systems to access the data from sensors that are already aboard regular vehicles. Such sensors include accelerometers, speed, odometer, and *conventional* global positioning system (GPS) receivers. The steady maturity of connected vehicles worldwide makes them an attractive platform to invent ways of using their existing on-board sensors to

monitor the condition of roadways. The typical vehicle does not integrate high-accuracy differential GPS (DGPS) receivers or any other special sensors that inertial profilers currently use to produce the IRI. Therefore, the main idea of this research is to use existing on-board sensors that will provide agencies with a more scalable and affordable alternative to the acquisition, maintenance, and operation of specially equipped inertial profiling vehicles that require highly trained personnel.

The transformation of inertial signals from the accelerometers aboard regular vehicles to produce roughness summary indices that are consistent with the IRI has been elusive, primarily because of sensitivities to the vehicle suspension response and the traversal speed (Du *et al.* 2014). To address this challenge, researchers developed and demonstrated a signal transform that modulates the road impact factor (RIF) with speed to produce a roughness index that is directly proportional to the IRI (Bridgelall 2014). The RIF-transform produces a representation of the true roughness that riders experience within a specified speed band and in actual vehicles versus simulated quarter-cars. A corresponding Time Wavelength-Intensity Transform (TWIT) combines the RIF-indices from all available speed bands to produce a speed-independent summary of roughness. The connected vehicle approach obviates the need for calibration with individual vehicle suspension behaviours by applying the central limit theorem to a large volume of data from different speed bands. Hence, the average RIF-index across all speed bands reflects the typical ride quality experienced at any speed, and establishes a practical figure-of-merit to trigger specific remediation responses.

The connected vehicle approach relies on *conventional* GPS receivers to tag the inertial samples with geospatial positions. Consequently, the precision in roughness localization that is achievable depends on the performance of the underlying GPS system. Administrators of the conventional GPS system expect that the six-sigma interval for horizontal position precision under direct line-of-sight conditions will be about ±6.7 meters, which is equivalent to a standard deviation of 2.2 meters about the mean (USDHS 1996). However, this uncertainty could increase to more than ±10 meters when multi-path reflections from buildings, large trees, and other tall structures distort the weak satellite signals.

This research extends the practice of using reflective tape markers to improve the precision of laser-based inertial profilers by substituting a reference anomaly for the accelerometer-based approach. The reference anomaly may be an artificial speed bump or an existing anomaly such as a pavement patch or rough joint at a pre-determined geospatial position. Hence, the main proposal of this paper is to avoid the use of GPS by instead using a reference anomaly of known geospatial position. That is, the segment origin will begin at the position of the reference anomaly. Practitioners must record its actual geospatial position on the path. This approach is analogous to the practice of placing a pneumatic tube sensor across known geospatial positions of the roadway to measure traffic volume. The speed sensor of the vehicle and a timer (instead of the GPS) will provide the information needed to calculate precise and continuous distance markers for the remaining inertial signal samples, relative to the path origin. The final implementation will rely on the speed sensor aboard a connected vehicle. However, the case study for this paper uses sensors from a smartphone to emulate the output of connected vehicle sensors because the authors did not have access to a standard connected vehicle. Incidentally, the smartphone implements the speed sensor by using its integrated GPS and inertial sensors. Therefore, the actual connected vehicle sensors will likely provide even better results than the case study demonstrates.

The main objective of this study is to quantify the relative precision and accuracy improvement in roughness localization and quantification by using reference inertial markers (RIM) instead of GPS receivers. Practitioners could use the GPS position tags for coarse localization of the approximate position of an anomaly detected in the inertial data stream, and then use the neighbouring path position tags to identify its precise position relative to the path origin.

The organization of this paper is as follows: the next section will develop a model to characterize the errors in position tagging and roughness measurement. The third section will describe the case study conducted to quantify statistics of the contributing factors that dilute the precision of position tagging. The fourth section will assess the difference in localization errors between the RIM and the GPS position tagging methods. The case study will demonstrate the utility of applying the RIM method to identify and

quantify the localized roughness of relatively small concrete panels for possible remediation or replacement. The final section will summarize and conclude the study.

2. Roughness measurement technique

This section reviews the connected vehicle method of inertial signal transformation that reports roughness in direct proportion to the IRI. Without access to an actual connected vehicle, the authors used a smartphone to log the equivalent sensor data that would have been available directly from the integrated vehicle systems. A model to characterize the localization errors also isolates the factors that dilute the precision. Simulations of quarter-car responses to bump traversals demonstrate how suspension transient responses contribute to localized roughness biases.

2.1. Inertial signal transformation

The RIF-transform produces a measure of localized roughness such that

$$R_{\bar{v}}^{L} = \sqrt{\frac{1}{L}\sum_{n=0}^{N-1}\left|g_{z[n]}v_n\right|^2 \delta t} \tag{1}$$

where the RIF-index $R_{\bar{v}}^{L}$ is the average g-force magnitude experienced per unit of distance L travelled. The vertical acceleration for signal sample n is $g_{z[n]}$ and the instantaneous traversal speed is v_n. For an average sample period of δt, the average spatial resolution achievable would be $\delta L = v_n\, \delta t$.

2.2. Roughness indices

For multiple traversals involving one or more vehicles, an ensemble average of the RIF-indices for a selected spatial resolution window produces an estimate of the segment roughness with ever-increasing levels of precision as the traversal volume increases. The ensemble average RIF-indices (EAR) is

$$\overline{R}_{\bar{\bar{v}}}^{L} = \frac{1}{N_{\bar{v}}}\sum_{\rho=1}^{N_{\bar{v}}} R_{\bar{v}}^{L}[\rho] \tag{2}$$

where $R_{\bar{v}}^{L}[\rho]$ is the RIF-index from the ρ^{th} traversal of the segment at an average speed of $\bar{v}$, and $\bar{\bar{v}}$ is the batch mean speed from all traversals of the segment. The number of available traversals for a speed band of average speed of $\bar{v}$ is $N_{\bar{v}}$. Tagging each vertical acceleration sample $g_{z[n]}$ with a geospatial

position and color-coding the EAR-index will produce a map-based visualization of the segment roughness. As the precision increases with additional traversals volume, the transition between smooth and rough segments will become sharper.

2.3. Geospatial position tagging

A smartphone application (app) dubbed pavement analysis via vehicle electronic telemetry (PAVVET) emulates the connected vehicle data that the RIF-transform converts to RIF-indices (Bridgelall 2015). Table 1 shows a fragment of the data from the PAVVET app and its format.

Table 1. Data format used for the RIF-transform.

Time	Gz	Lat	Lon	Vel	Pitch	Roll	Yaw	Gx	Gy
21.347	-0.98	46.88096	-96.7701	1.42	8.19	1.51	-25.61	0.05	-0.13
23.956	-1.02	46.88096	-96.7701	1.42	8.17	1.51	-25.63	0.05	-0.14
26.118	-0.99	46.88096	-96.7701	1.42	8.17	1.51	-25.63	0.02	-0.15
37.812	-1.03	46.88096	-96.7701	1.42	8.17	1.50	-25.64	0.05	-0.12
48.627	-0.97	46.88096	-96.7701	1.42	8.17	1.50	-25.64	0.08	-0.14
59.410	-1.02	46.88096	-96.7701	1.42	8.16	1.55	-25.67	0.00	-0.16
123.741	-0.95	46.88096	-96.7701	1.42	8.20	1.47	-25.73	0.02	-0.13
134.777	-1.05	46.88096	-96.7701	1.42	8.20	1.47	-25.73	0.04	-0.15

The first row contains a header with labels for each column of data sampled from the sensors. The “Time” column is the sample period in milliseconds. The accelerometer produced the “Gz,” “Gx,” and “Gy” inertial signals, which are the acceleration levels sensed in the vertical, lateral, and longitudinal directions, respectively. The values are in units of g-forces. The gyroscope produced the “Pitch,” “Roll,” and “Yaw,” which are the sensor orientation angles in degrees, respectively. The post-processing algorithm uses a three-dimensional rotation matrix to extract the resultant vertical acceleration, regardless of the orientation of the smartphone (Bridgelall 2014).

The GPS receiver produced the “Lat” and “Lon,” which are the latitude and longitude, respectively, in decimal format. The GPS receiver also produced the “Vel,” which is the estimated ground speed in $\mathrm{m\,s^{-1}}$. The fastest update rate achievable for the GPS receiver of the iPhone® 4S used is

approximately 1 Hertz. The maximum update rate obtained from the accelerometer was somewhat greater than 100 Hertz (Apple Inc. 2014). The GPS receiver utilizes inertial navigation system (INS) and Kalman filtering techniques to produce speed updates at a rate that matches the accelerometer update intervals. This technique smooths out gaps from loss of GPS satellite signals such as when traveling through a tunnel or urban areas with poor satellite signals reception (Groves 2013). The algorithm to produce geospatial position tags interpolate between successive GPS position updates to associate each inertial sample with a path distance. This approach produces path distance tags with greater accuracy, particularly for curvilinear paths and turns. Another benefit is that tagging based on speed and time fills in path distance gaps that result when the GPS receiver loses line-of-sight conditions. The distance from any GPS position update υ_0 is

$$\upsilon_\rho = \upsilon_0 + \sum_{n=1}^{\rho} v_n \delta t_n \tag{3}$$

where υ_ρ is the position of the ρ^{th} inertial sample update.

2.4. Position tagging error

For the case of an isolated bump, the position tag $\hat{\upsilon}_p$ of the first peak in the inertial response signal is an estimate of the true position υ_p of the bump's peak. The estimate includes distance biases such that

$$\hat{\upsilon}_\mathrm{p} = \upsilon_p + \left(\bar{\varepsilon}_\mathrm{DSP} + \bar{\varepsilon}_\mathrm{i}\right) + \bar{\varepsilon}_\mathrm{b} + \left(\bar{\varepsilon}_\mathrm{s} + \bar{\varepsilon}_\mathrm{GPS}\right) \tag{4}$$

This expression groups the biases into three categories: signal processing, vehicle response, and GPS receiver related. The position bias from digital signal processing (DSP) is the expected delay $\bar{\varepsilon}_\mathrm{DSP}$ from digital filtering, and $\bar{\varepsilon}_\mathrm{i}$ is the error in locating a peak within the interpolation sub-interval. The vehicle mechanical response delay $\bar{\varepsilon}_\mathrm{b}$ depends on the quarter-car parameters, the bump width, and the traversal speed. The GPS receiver related biases are its average longitudinal position $\bar{\varepsilon}_\mathrm{s}$ of installation in the vehicle relative to the first axle, and the average offset in position tag $\bar{\varepsilon}_\mathrm{GPS}$.

For a given test vehicle, variances in the signal processing bias are negligible and the sensor position bias will remain unchanged. Hence, variances in the phase response of the vehicle suspension system and randomness in GPS position estimates will dominate the position tagging errors. Previous work established that phase response variations in the suspension system of a given vehicle accounted for less than one-centimetre of the variations observed in the position tags (Bridgelall 2015). Therefore, the error magnitude that excludes GPS randomness is comparable to the error of laser-based inertial profilers that standardize on a sample interval of 25-millimeters (~1 inch) (Perera and Elkins 2013).

The geospatial position tag $\bar{\varepsilon}_{\text{GPS}}$ reported by the GPS receiver and its associated embedded system consists of two error components such that the average position bias is

$$\bar{\varepsilon}_{\text{GPS}} = \bar{\varepsilon}_{\text{dGPS}} + \bar{\varepsilon}_{\text{dlag}} \tag{5}$$

The mean geospatial position bias from trilateration is $\bar{\varepsilon}_{\text{dGPS}}$ and the mean latency in applying position tags is $\bar{\varepsilon}_{\text{dlag}}$. The former is normally distributed with zero mean (Gade 2010). Hence, the position bias becomes $\bar{\varepsilon}_{\text{GPS}} = \bar{\varepsilon}_{\text{dlag}}$. From equation (5), the total variance in geospatial position tagging σ^2_{GPS} is

$$\sigma^2_{\text{GPS}} = \sigma^2_{\text{dGPS}} + \sigma^2_{\text{dlag}} \tag{6}$$

The variance σ^2_{dGPS} in geospatial position estimates from GPS trilateration can be several meters to tens of meters, depending on the signal reception conditions as previously described. The latency in position tagging $\bar{\varepsilon}_{\text{dlag}}$ is

$$\bar{\varepsilon}_{\text{dlag}} = \bar{\tau}_{\text{lag}}\bar{v}. \tag{7}$$

A previous study determined that the performances of the GPS receiver processing chain and the host platform for the embedded GPS system accounts for the magnitude of the average latency in position tagging $\bar{\tau}_{\text{lag}}$ (Bridgelall 2015). The corresponding variance in tag distance lag σ^2_{dlag} is

$$\sigma^2_{\text{dlag}} = \left(\bar{v}\sigma_{\tau\text{lag}}\right)^2 + \left(\bar{\tau}_{\text{lag}}\sigma_v\right)^2 \tag{8}$$

where σ_v^2 is the variance in vehicle speed. Lag time variances $\sigma_{\tau lag}^2$ typically occur within one or two GPS update intervals.

2.5. Localized roughness bias

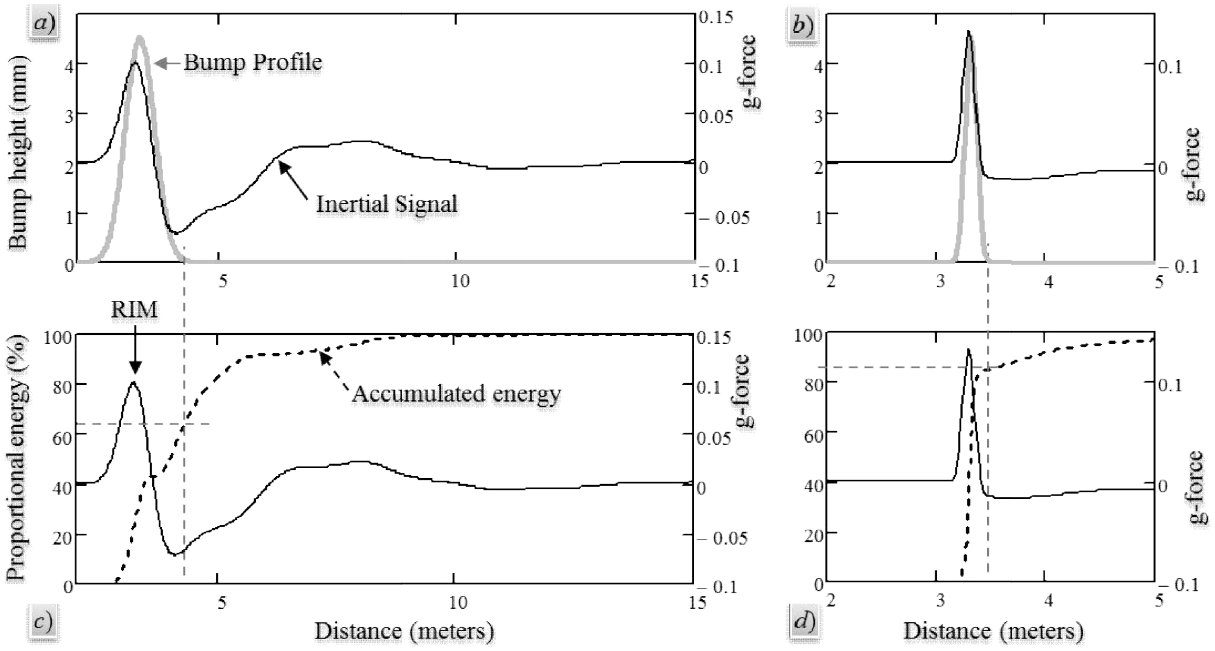

Figure 1. Quarter-car inertial response from wide and narrow bump traversals.

An anomaly will produce at least one maxima in the inertial signal. Figure 1 compares the simulated inertial signal from traversing relatively wide and narrow isolated bumps at the speed of 67 km h^{-1} (~42 mph). The simulated inertial signal is a mathematical convolution of the quarter-car model and the vertical acceleration from traversing the elevation profile. The bump profile is a modified Gaussian radial bases function, and the quarter-car parameters are estimates based on a technique described in previous research (Bridgelall 2014). Table 2 compares the quarter-car parameters for the vehicle used in the case study presented later and the Golden Car.

Table 2. Parameters for the Golden Car and the case study vehicle.

Parameter	Golden Car	2011 Chevy Traverse
Sprung-mass natural frequency (Hertz)	1.27	2.51
Sprung-mass damping ratio	0.38	0.41
Unsprung-mass natural frequency (Hertz)	10.50	10.48
Unsprung-mass damping ratio	0.05	0.09

The position of the bump in Figure 1 is at a wheelbase distance of 3.3-meters from the origin. Figure 1a and 1b shows the g-forces that the equivalent quarter-car produces during and after traversing a 1.8-meter (6-feet) and a 0.3-meter (1-foot) wide bump, respectively. The bump height is 4.5 millimetres. Figures 1c and 1d plots their respective proportional roughness energy accumulated as a function of distance. It is evident that most of the energy accumulates during the bump traversal and the remaining energy dissipates during the transient response after the vehicle crosses the bump.

Given the specific quarter-car, the amount of roughness energy that accumulates during the bump traversal is a function of speed and the bump width. Figure 2a plots the proportional roughness energy accumulated after traversing bumps with three different widths, as a function of speed. It is evident that for all cases, at least 60% of the roughness energy will accumulate during a bump traversal.

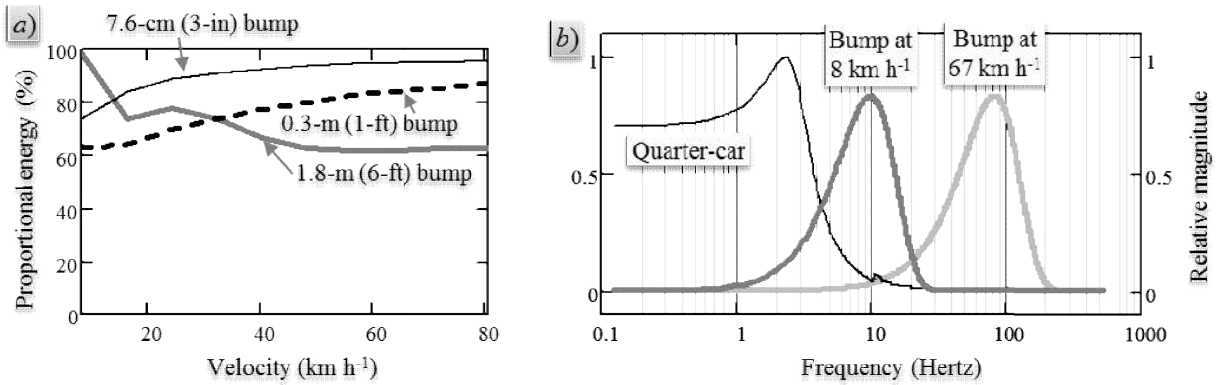

Figure 2. Bump energy as a function of traversal speed.

The non-linear behaviour with speed stems from the non-linear transfer-function of the quarter-car. In general, bump energy that translates with traversal speed to coincide with the unsprung-mass mode near 10 Hertz amplifies the quarter-car response, which extends the transient response beyond the

duration of the bump profile. For example, figure 2b shows the frequency response of the vertical acceleration energy that the 0.3-meter wide bump produced when the vehicle traversed it at 8 km h^{-1} and 67 km h^{-1}, respectively. Traversing the bump at a lower speed moves the peak vertical acceleration energy from 90 Hertz to 10 Hertz. As implied in figure 2a, the vertical acceleration energy of the 1.8-meter wide bump translates from a lower frequency to the 10-Hertz region when the speed exceeds 40 km h^{-1}. Subsequently, any vibrations that sustain after the trailing edge of an anomaly will result in a roughness bias for the segment that immediately follows.

3. Case studies

This section describes the case study setting and the layout of the concrete panels. A histogram of the GPS position tags of the RIM expresses their statistical distribution.

3.1. Test facilities

The Minnesota Road Research Facility (MnROAD) is an outdoor research laboratory that the Minnesota Department of Transportation operates in the U.S. to test different types of pavement (MnROAD 2015). Cell 40 (figure 3a), repaved in early 2013 with 80 concrete panels along each wheel path, has a total length of 152.4-meters (500-ft). As seen in figure 3b, the square Portland Cement Concrete (PCC) panels are approximately 1.8-meter (6-ft) long. The cell begins with an asphalt pavement section and then transitions into the PCC panels (figure 3c). The uneven joint between the asphalt and the PCC sections produced the desired RIM that was easy to detect after applying a low-pass filter with a cut-off frequency of 2-hertz.

Without access to an actual connected vehicle for this case study, a smartphone with the PAVVET app aboard of a 2011 Chevy Traverse (figure 3b) logged the equivalent sensor data that would have been available directly from the integrated vehicle systems. The app ran on three smartphones secured flat with tape to the hatchback trunk deck. The installation choice assured maximum contact of the smartphone with the body of the vehicle for vibration sensing, and a direct line-of-sight to the GPS satellites to assure data quality. There were 18 traversals at a batch mean speed of approximately 67 km h^{-}

[1]. Hence, the app collected 54 data streams for post processing. The mean inertial sample rate and the mean GPS update interval were 93 Hertz and 0.97 seconds, respectively.

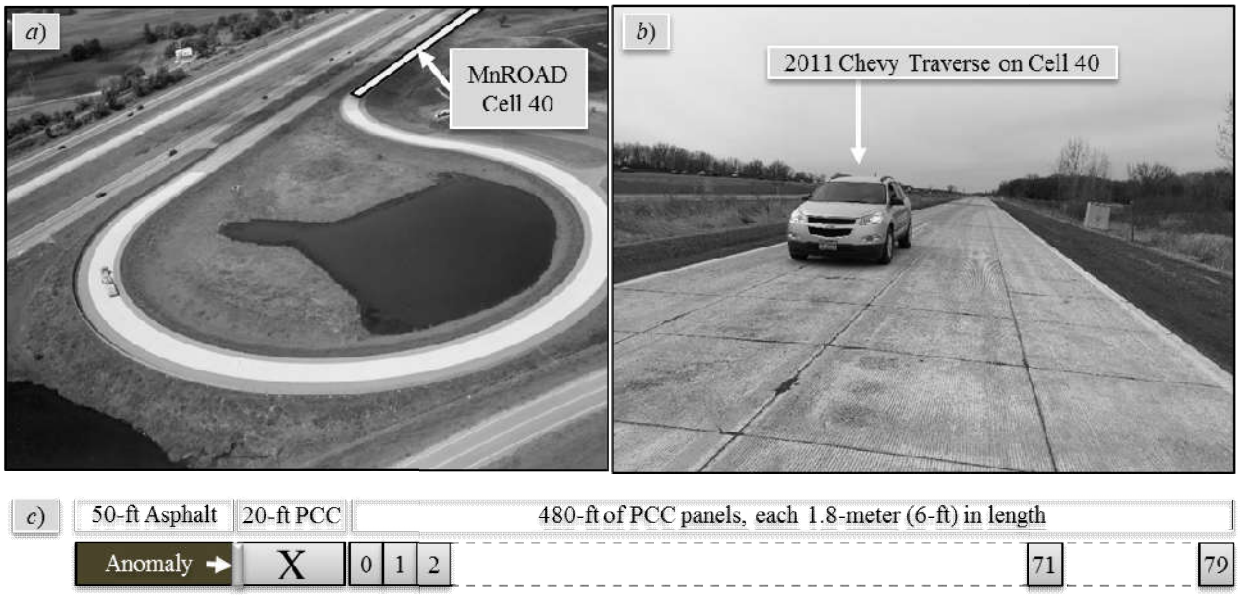

Figure 3. Test site and concrete panel configuration.

3.2. Distribution of position tags

Figure 4a plots the inertial signal for two randomly selected data streams. The signal shape that contains the RIM is a response that is familiar from the simulated bump traversal (figure 1). It is evident that the RIM position tags vary significantly among traversals. The RIF-transform with a spatial resolution window equal to a panel length (1.8-meters) produced the associated sequence of RIF-indices shown for the first inertial signal (figure 4a).

Figure 4b plots the EAR using equation (2) with the same spatial resolution window. The EAR reveals a multi-modal distribution of the position tags that is easiest to observe about the EAR maxima. A least squares fit of the Gaussian distribution around the first EAR (between the position markers φ and ψ) exhibited a significance value of 99.85% for the chi-squared test statistic (χ^2)

$$\chi^2 = \sum_{k=1}^{n} \frac{(O_k - E_k)^2}{E_k}. \tag{9}$$

The random variables O_k are the histogram values observed in bin k and E_k are the expected values of the

hypothesized distribution. The chi-squared test cannot reject the hypothesis that the position tags follow a Gaussian distribution because the significance value is much greater than 5%. Figure 3d is an enlarged view of the Gaussian fit about the first maxima of the EAR.

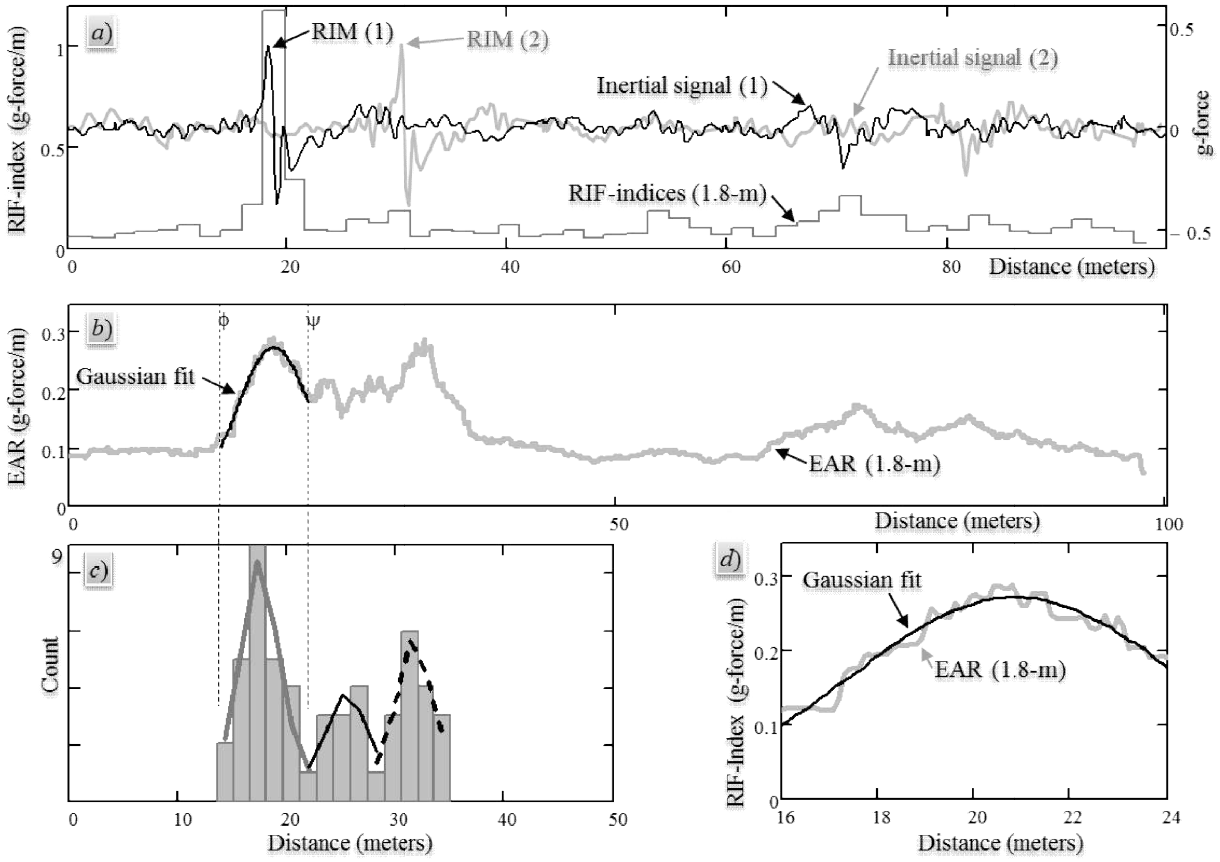

Figure 4. RIF-indices and their position distribution.

Figure 4c is a histogram of the GPS position tags for the RIM of all traversal. The tri-modal distribution observed corresponds to the three independent GPS receivers used. The plots show a least squares fit to each mode of the histogram, and table 3 summarizes the parameter estimates.

The χ^2 significance listed for the Gaussian and the t-distribution fits for each mode are significantly larger than 5%. The degrees of freedom used to calculate the χ^2 significance is one less than the number of histogram bins, minus the two independent (amplitude and mean) parameter estimates. Hence, these chi-squared tests cannot reject the hypothesis that the position tags for the RIM follow either

the Gaussian or the t-distributions. The strong agreement with classic distributions indicates that the dominant error contributors distribute normally as expected.

Table 3. Parameters of the least-squares distribution fit.

Parameter	Mode 1	Mode 2	Mode 3
Mean (meters)	17.49	25.45	31.66
Standard deviation (meters)	1.92	2.29	1.96
Degrees-of-freedom	3	2	2
χ^2 significance for the Gaussian (%)	82.58	72.69	82.14
χ^2 significance for the t-distribution (%)	80.95	65.65	76.77

Retagging the data stream by setting the RIM of each inertial signal as the origin υ_0 and using equation (3) to produce position tags for all the other inertial samples eliminated the observed variations from GPS position tagging. Hence, the remaining uncertainty in localization is a function of the errors in measuring the instantaneous speed and the accelerometer update intervals. Previous work established that those errors are sub-millimetre based on the application of Kalman filtering and longitudinal acceleration sensing to estimate the instantaneous speed (Bridgelall 2015).

4. Results and discussion

From table 3, the batch mean of the standard deviations of the RIM position tags from each smartphone is 2.1 meters. This result closely matches the standard deviation of 2.2 meters that GPS operators expect under nominal conditions. The largest difference in RIM position tag bias among smartphones was (31.66 – 17.49) = 14.17 meters. At the average speed of the vehicle, this distance bias corresponds to 0.76 seconds, which is well within one GPS update interval.

Using a spatial resolution window of 1.8-meter for the RIF-transform, figure 5 compares the EAR for the GPS-tagged and the RIM-aligned inertial samples. It is evident that in addition to delaying the localized roughness of the reference anomaly, the random distribution of the GPS position tags smears the localized roughness measurements. Therefore, relative to the RIM-aligned method, the EAR-indices of the GPS-tagged method could result in more than a two-fold error in measuring the localized roughness of a PCC panel. However, the roughness measurement error of the GPS-tagged method will match those of

the RIM-aligned method as the size of the spatial resolution window increases well beyond the uncertainty interval of the GPS position estimates.

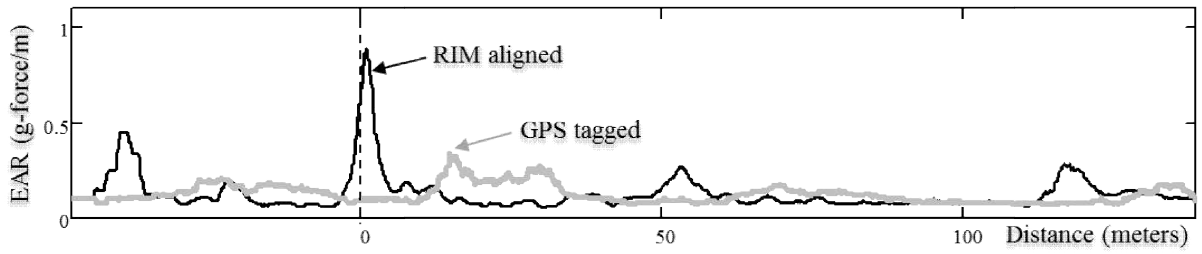

Figure 5. The EAR for the RIF-transform of GPS-tagged and RIM-aligned inertial samples.

The minimum length of that window must exceed the bias and variations from GPS position tagging such that

$$L \geq \bar{\varepsilon}_{dlag} + 3\sigma_{GPS}. \tag{10}$$

The last factor is the right half of a six-sigma interval for the GPS uncertainty interval. Substituting equation (7) and an average lag time as the midpoint of one GPS update interval τ_{GPS} such that $\bar{\tau}_{\text{lag}} = 0.5\tau_{\text{GPS}}$ yields a recommended spatial window of

$$L \geq \frac{\tau_{\text{GPS}}}{2}\bar{v} + 3\sigma_{\text{GPS}}. \tag{11}$$

Using the estimates from the third smartphone (table 3) as a case study, the recommended spatial resolution for the GPS tagged method should be greater than (0.97/2)(18.61) + 3(1.96) ≈ 15 meters. Most practitioners use a much larger spatial resolution of approximately 161-meters (0.1 mile) to characterize and report pavement smoothness (Merritt *et al*. 2014). Equation (11) provides an additional insight that the anticipated spread in GPS position estimates will become dominant when the GPS update interval is set below approximately 0.5 seconds, or when the instrumented vehicle travels slower.

Table 4 demonstrates the improvement in measurement agreement between the RIM-aligned and GPS-tagged methods when using longer spatial resolution windows for the EAR.

Table 4. Distribution of RIF-indices for different segment lengths.

EAR Window	GPS-Tagged		RIM-Aligned	
	$\overline{R}_{\bar{v}}^{L}$	σ_R^L	$\overline{R}_{\bar{v}}^{L}$	σ_R^L
40 meters	0.340	0.021	0.340	0.020
60 meters	0.291	0.018	0.293	0.017
80 meters	0.272	0.021	0.270	0.016
100 meters	0.271	0.016	0.271	0.015

The reference anomaly is at the centre of the window for each case, therefore, the EAR decreases with increasing window lengths as observed in the table. The standard deviations also decrease for each method because measurement errors spread across a longer spatial window. As expected, the standard deviation of roughness measurements is slightly smaller for the RIM-aligned method, but the gap closes as the window length increases.

The margin-of-error (MOE) for the distribution of RIF-indices $\Delta R_{1-\alpha}^{L}$ within a (1-α)% confidence interval with significance α (Papoulis 1991) is

$$\Delta R_{1-\alpha}^{L} = \pm \frac{\sigma_R^L \times t_{1-\alpha/2,df}}{\sqrt{N_{\bar{v}}}} \tag{12}$$

where $t_{1-\alpha/2,df}$ is the *t*-score for a normalized cumulative *t*-distribution with *df* degrees of freedom. The standard deviation of the RIF-index is denoted σ_R^L. The ratio of $MOE_{1-\alpha}$ to the EAR is the MOE percentage, which is a relative measure of the amount of measurement spread about the mean value. For this case study, the $MOE_{0.95}$ (%) for the 100-meter segment indicates that 95% of the RIF-indices will be within 1.7% and 1.5% of the mean for the GPS-tagged and the RIM-aligned methods, respectively. In conclusion, further increasing the length of the spatial resolution window of the EAR will absorb the effects of random GPS position tagging.

Using a spatial resolution that is equal to the panel-width, figure 6a plots the localized EAR-indices for each PCC panel using the RIM-aligned method.

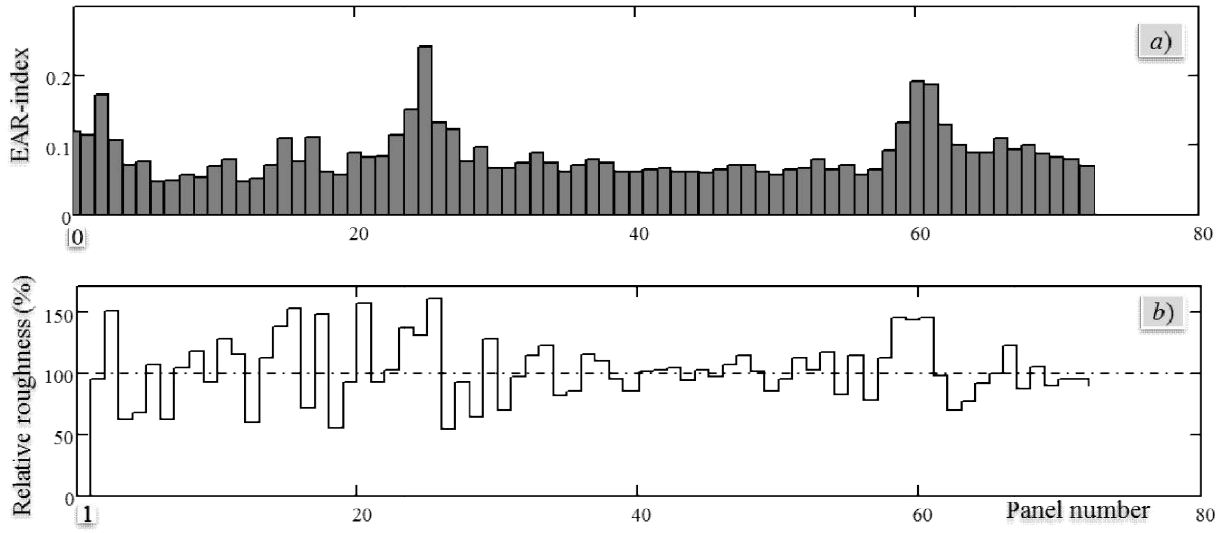

Figure 6. EAR and relative roughness for the Cell 40 concrete panels.

As simulated earlier (figure 2), the worst-case bump width will cause the vehicle to experience approximately 40% of the bump energy that a panel produced after traversing it. At the mean traversal speed, the transient response for a worst-case bump width will dissipate after traversing approximately eight panels. Therefore, the average overestimation of roughness per panel, in the worst case, will be no greater than 40/8 = 5%. However, the vehicle experiences such latent roughness while traversing every panel. Hence, the ratio of roughness change relative to the preceding panel produces a more accurate view of the relative roughness experienced per panel. Figure 6b shows the roughness change in percentage from a panel relative to the preceding panel. Any abrupt deviation in roughness from the 100% level is an indication of the relative impacts from localized roughness.

5. Summary and conclusions

Affordable and scalable methods of measuring localized roughness enable improved efficiencies and effectiveness in the practice of roadway asset management. However, the prevalent approach that relies on laser-based inertial profilers is relatively expensive to deploy network wide for continuous evaluations. Connected vehicle methods that use the accelerometers and conventional GPS receivers aboard regular vehicles provide an attractive alternative, but the dilution of precision of the conventional system limits

the achievable precision in localization to a few tens of meters.

This research examined the relative improvement in precision of roughness localization achievable by using a reference anomaly in the traversal path to produce reference maxima in the inertial signal, and position tag offsets based on the sample intervals and the instantaneous speed. The associated case study utilized the MnROAD facilities to demonstrate that sub-centimetre precision in localization is achievable. Furthermore, the method provides a nominal two-fold improvement in the accuracy of measuring localized roughness. However, both methods provide similar accuracy levels in localized roughness estimation when the spatial resolution exceeds the GPS-related interval of uncertainty. The case study revealed that when reporting roughness for segment lengths that are typical of the IRI, for instance 0.1-kilometres, the margin-of-error in roughness measurements will diminish below 2% as the number of traversal samples exceeds 50.

The case study used a smartphone to emulate a single connected vehicle to demonstrate an application of the method using reference inertial markers by localizing the roughness of relatively small Portland Cement Concrete panels. A sharp change in the relative roughness between the 1.8-meter concrete panels identified localized roughness. Although the speed estimates from the smartphone are not certified based on national standards, the proposed method provided acceptably consistent characterizations of the pavement roughness. Therefore, the data from certified sensors of an actual connected vehicle would likely provide even greater data quality to further boost the performance of the proposed method.

The authors are currently collaborating with the MnROAD facility to analyse strain changes within select concrete panels. Ongoing research will utilize the method of reference inertial markers to isolate and compare the ratios of panel roughness with the corresponding ratios of the strain sensor output. Subsequently, this data will support future research that will examine the link between roughness progression and temporal changes in the pavement strain.

Acknowledgement

A grant from the Mountain Plains Consortium supported this research. The authors graciously thank the

MnROAD technicians who provided access and technical support for the data collection.

References

Ahlin K and Granlund N J 2002 Relating road roughness and vehicle speeds to human whole body vibration and exposure limits *Int. J. Pavement Eng.* **3** 207-216

Apple Inc. 2014 *Location and Maps Programming Guide* (Cupertino: Apple Inc.)

Bridgelall R 2014 A participatory sensing approach to characterize ride quality *Proc. SPIE 9061* (San Diego: SPIE)

Bridgelall R 2014 Connected vehicle approach for pavement roughness evaluation *J. Infrastruct. Syst.* **20** 04013001.1-04013001.6

Bridgelall R 2015 *Pavement Performance Evaluation Using Connected Vehicles* (Fargo: North Dakota State University)

Bridgelall R 2015 Precision bounds of pavement distress localization with connected vehicle sensors *J. Infrastruct. Syst*. **21** 04014033.1-04014033.7

Chen D and Dye M 2014 Evaluation of initial IRI values as acceptance criteria for flexible pavements *Int. J. Eng. Res. Innov.*, **6**

Du Y, Liu C, Wu D and Jiang S 2014 Measurement of International Roughness Index by using z-axis accelerometers and GPS *Math. Probl. Eng.* **2014** 1-10

Gade K 2010 A non-singular horizontal position representation. *J. Navigation* **63** 365-417

Gillespie T D, Sayers M W and Queiroz C A V 1986 *The International Road Roughness Experiment: Establishing Correlation and Calibration Standard for Measurement* (Washington, D.C.: The World Bank)

Groves P D 2013 Principles of GNSS, *Inertial, and Multisensor Integrated Navigation Systems* (Norwood: Artech House)

Harrison F and Park H -A 2008 *Comparative Performance Measurement: Pavement Smoothness* (Washington D.C.: NCHRP)

Karamihas S M and Senn K 2012 *Curl and Warp Analysis of the LTPP SPS-2 Site in Arizona* (Washington, D.C.: Federal Highway Administration)

Lak M A, Degrande G and Lombaert G 2011 The influence of the pavement type on ground-borne vibrations due to road traffic *EURODYN 2011* (Leuven: Ku Leuven) 777-784

Merritt D K, Chang G K and Rutledge J L 2014 *Best Practices for Achieving and Measuring Pavement Smoothness: A Synthesis Of State-Of-Practice* (Baton Rough: Louisiana Transportation Research Center)

MnROAD 2015 *Safer, Smarter, Sustainable Pavements through Innovative Research* (Monticello: Minnesota Department of Transportation)

NCHRP 2013 *Measuring, Characterizing, and Reporting Pavement Roughness of Low-Speed and Urban Roads* (Washington, D.C.: NCHRP)

Papagiannakis A T 1997 *The Need for a New Pavement Roughness Index; RIDE* (Washington, D.C.: Society of Automotive Engineers International)

Papoulis A 1991 *Probalility, Random Variables, and Stochastic Processes* (New York: McGraw-Hill)

Perera R W and Elkins G E 2013 *LTPP Manual for Profile Measurements and Processing* (Washington, D.C.: Federal Highway Administration)

USDHS 1996 *NAVSTAR GPS User Equipment Introduction* (Washington, D.C.: U.S. Department of Homeland Security)

USDOT 2015 *Connected vehicle pilot deployment program* (Washington, D.C.: U.S. Department of Transportation)